Electronic Spectroscopy and Photodissociation Dynamics of the 1-Hydroxyethyl Radical CH$_3$CHOH

Boris Karpichev, Laura W. Edwards, Jie Wei, and Hanna Reisler*

Department of Chemistry, University of Southern California, Los Angeles, California 90089-0482

Received: September 7, 2007; In Final Form: October 30, 2007

The electronic spectroscopy and photodissociation dynamics of the CH$_3$CHOH radical in the region 19 400−37 000 cm^{-1} (515−270 nm) were studied in a molecular beam using resonance-enhanced multiphoton ionization (REMPI), photofragment yield spectroscopy, and time-of-flight (TOF) spectra of H and D fragments. The onset of the transition to the Rydberg 3s state, the lowest excited state, is estimated at 19 600 $\pm$ 100 cm^{-1}. The 3s state dissociates fast, and no REMPI spectrum is observed. The origin band of the transition to the 3p$_z$ state, identified by 2 + 2 REMPI, lies at 32 360 $\pm$ 70 cm^{-1}, and a vibrational progression in the C−O stretch is assigned. When exciting CH$_3$CHOH near the onset of the unstructured absorption to the 3s state, only one peak is observed in the center-of-mass (c.m.) translational energy (E_t) distribution obtained by monitoring H photofragments. The measured recoil anisotropy parameter $\beta = -0.7 \pm 0.1$ is typical of a perpendicular transition. The O−H bond energy is determined to be $D_0 = 1.1$ eV ± 0.1 eV. At excitation energies >31 200 cm^{-1} (3.87 eV) a second, low E_t peak appears in the c.m. E_t distribution with $\beta \approx 0$. Its relative intensity increases with excitation energy, but its β value does not change. In contrast, the β value of the higher E_t peak becomes monotonically less negative at higher excitation energies, decreasing to -0.2 ± 0.1 at 35 460 cm^{-1}. By comparison of the TOF distributions of the isotopologs CH$_3$CHOH, CH$_3$CHOD, and CD$_3$CHOH, it is concluded that two major product channels dominate the photodissociation, one leading to acetaldehyde and the other to vinyl alcohol (enol) products. There is no indication of isomerization to ethoxy. It appears that separate conical intersections lead to the observed channels, and the dynamics at the conical intersection and the exit channel deposit much of the available energy into internal energy of the products.
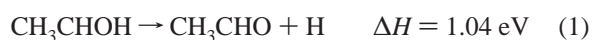
I. Introduction

The chemistry of hydroxyalkyl radicals is important in atmospheric chemistry and combustion environments. For example, CH$_2$OH is a significant product in the reaction of O(^{1}D) with methane[1−5] and of Cl atoms and OH radicals with methanol.[6−9] Of the hydroxyalkyl radicals larger than CH$_2$OH, the structural isomers 1- and 2-hydroxyethyl radicals (CH$_3$-CHOH and CH$_2$CH$_2$OH, respectively),[10−14] are relevant to ethanol combustion. These isomers are also involved in the photochemistry of the ethoxy radical[15,16] as products in the reaction of halogen atoms with ethanol[6,9−11,13,17] and as intermediates in the O + C$_2$H$_5$ and OH + C$_2$H$_4$ reactions.[18−22] The role of hydroxyalkyl intermediates in combustion reactions has recently been highlighted by the discovery that the enol tautomers of aldehydes are significant combustion intermediates. For example, vinyl alcohol (ethenol, CH$_2$=CHOH), the less stable tautomer of acetaldehyde (CH$_3$−HC=O), is formed in flames of ethanol, olefins, and commercial fuels.[23] Both tautomers can be formed in the decomposition of ground state hydroxyethyl radicals.[18,21] In spite of their importance very little is known about the photophysics and photochemistry of hydroxyalkyl radicals.

An unstructured electronic absorption spectrum of CH$_3$CHOH recorded at 300 K in the region 230−300 nm has a maximum absorption cross section of 3.6 $\times$ 10^{-18} cm^2.[10] The spectrum shows that absorption at <300 nm rises strongly toward shorter wavelengths, but the measurements stopped at 230 nm, where

the spectrum reached a plateau, and did not extend to wavelengths longer than 300 nm. A paper on the kinetics of CH$_3$-CHOH reports a resonance-enhanced multiphoton ionization (REMPI) signal of the parent ion in the range 430−460 nm,[24] which likely arises from 2 + 1 ionization via a Rydberg state. The adiabatic ionization energy of CH$_3$CHOH is 6.64 eV,[13,25] much lower than the corresponding value for CH$_2$OH (7.56 eV).[26] A photoelectron spectroscopy study revealed a progression of ∼1600 cm^{-1} in the CO stretch of the ion, in agreement with the expected shortening of the CO bond upon ionization.[25]

The photodissociation of the hydroxyethyl radical has not been studied before. However, following UV excitation of the ethoxy isomer (CH$_3$CH$_2$O), Neumark and co-workers observed the unexpected C$_2$H$_3$ + H$_2$O channel, which they suggested evolved via isomerization on the excited-state to hydroxy-ethyl.[15,16]

There are no theoretical papers on the excited states of the hydroxyethyl radical. However, there are several ab initio calculations of the geometry of the ground state and the ion as well as barriers to isomerization and dissociation on the ground-state potential energy surface (PES).[12,14,18,21] The lowest barrier channels calculated for the ground state PES are:[21,27]

$$CH_3CHOH \rightarrow CH_3CHO + H \qquad \Delta H = 1.04 \text{ eV} \quad (1)$$

$$\rightarrow CH_2CHOH + H \quad \Delta H = 1.46 \text{ eV} \quad (2)$$

$$\rightarrow CH_3 + CHOH \qquad \Delta H = 3.13 \text{ eV} \quad (3)$$

where ΔH is the thermochemical dissociation threshold.

---

* To whom correspondence should be addressed. E-mail: reisler@usc.edu.

The 1-Hydroxyethyl Radical CH₃CHOH

J. Phys. Chem. A, Vol. 112, No. 3, 2008 **413**

TABLE 1: Comparison of Energies and Quantum Defects of Rydberg States for CH₂OH and CH₃CHOH (δ is Obtained from the Experimental Results)

|	hydroxymethyl (CH₂OH)		1-hydroxyethyl (CH₃CHOH)		
state	T_0^E, cm^{-1} (eV) experiment[a]	δ	T_0^E, cm^{-1} (eV) estimated	T_0^E, cm^{-1} (eV) experiment	δ
3s	25 971 (3.22)	1.23	18 527 (2.29)	19 600 (2.43)	1.20
3p$_x$	35 004 (4.34)	0.94	27 695 (3.43)		
3p$_z$	41 053 (5.09)	0.65	33 684 (4.18)	32 360 (4.01)	0.73

[a] References 33−35.

The molecular elimination channels, CH₃CO + H₂ and CH₃ + CO + H₂, involve high barriers and tight TS's and, as in CH₂-OH, may not be competitive with simple bond fission channels.[28,29] In addition, the CH₃CH₂O ↔ CH₃CHOH isomerization can lead to CH₂O + CH₃ (ΔH = 0.85 eV) and CH₃CHO + H.[21] The barrier to isomerization is calculated at 1.61 eV from the hydroxyethyl side.[21]

In this paper, we present the first study of the photophysics and photochemistry of the 1-hydroxyethyl radical (CH₃CHOH) in a molecular beam in which we: (i) identify and assign its lowest electronic transitions; (ii) discuss the role of nonadiabatic transitions following electronic excitation in the region of the lowest Rydberg states; and (iii) identify dissociation pathways.

In interpreting the results we rely on information gained from similar studies on the prototype hydroxymethyl radical.[28−37] For example, the energies of the 3s and 3p Rydberg states of CH₃-CHOH are predicted by using the Rydberg formula with quantum defects δ similar to those of CH₂OH (see section IV and Table 1). Likewise, theoretical studies of CH₂OH photodissociation have shown that the lowest states are all Rydberg states and there are efficient couplings via conical intersections to the ground PES followed by fast dissociation,[31,32,36,37] and we expect that these would be important in CH₃CHOH as well. In particular, the out-of-plane modes involving the methyl group are likely to increase the efficiency of nonadiabatic couplings relative to CH₂OH, and this may account for the lack of structure in the 300 K absorption spectrum. Many radicals have low ionization energies and consequently low-lying Rydberg states. Rydberg−Rydberg and Rydberg−valence interactions are of fundamental importance to the photochemistry of these radicals.

II. Experimental Details

The experimental apparatus and procedures have been described in detail elsewhere, and here we elaborate only on procedures that have changed.[28,30,33] The radical is produced efficiently by the reaction of Cl with ethanol, where the more stable 1-hydroxyethyl radical, CH₃CHOH, is produced with 95% yield.[6,9,17]

$$CH_3CH_2OH + Cl \rightarrow HCl + CH_3CHOH$$
$$\Delta H = -10.7 \text{ kcal mol}^{-1} \tag{4}$$
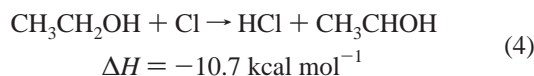
A mixture of 2.6% CH₃CH₂OD, CD₃CH₂OH (99.5 and 99.0%, respectively, Aldrich, used without further purification) or CH₃-CH₂OH (99.98% AAPER Alcohol, used without further purification), and ~1% Cl₂ (Matheson Tri Gas, high purity) in He at 2 atm total pressure is prepared in a 4-L glass bulb. A piezoelectrically driven pulsed nozzle operating at 10 Hz introduces this mixture to the source region of the differentially pumped vacuum chamber. Cl₂ is photodissociated by 355-nm radiation from a Nd:YAG laser (Spectra Physics, GCR-11; 5 mJ, focused by a 30 cm focal length (f.l.) cylindrical lens) directed at the edge of a 4 mm long quartz tube attached in front of the nozzle orifice. Cl atoms react with CH₃CH₂OH (CH₃CH₂OD, CD₃CH₂OH) to create CH₃CHOH (CH₃CHOD, CD₃CHOH).

Radicals generated in the quartz tube undergo cooling during the supersonic expansion. The rotational temperature is estimated at 10−15 K, as shown in our work with CH₂OH.[30] The detection chamber is separated from the source chamber by a skimmer (Beam Dynamics, 1.51 mm diameter). In the detection chamber, the pump and probe laser beams are counterpropagating and cross the molecular beam at a right angle.

The pump (dissociation) radiation is generated by a Nd:YAG-pumped OPO/OPA laser system (Continuum, PL8000/Sunlite/FX-1; 0.5−2 mJ at 250−400 nm, 14−20 mJ at 470−520 nm; 25 cm f.l. lens). The probe laser detects H and D fragments by 1 + 1′ REMPI via the Lyman-α transition. The doubled output (365 nm, 2 mJ) of a Nd:YAG-pumped dye laser system (Continuum, NY81/ND6000, LDS 751) is focused (20 cm f.l. lens) into a 1000 Torr mixture of Kr (25%) and Ar (75%). The tripled 121.6-nm radiation is focused in the detection chamber (MgF₂ 7.5 cm f.l. lens) along with the residual 356-nm light.

Ions generated in the experiment are accelerated perpendicularly to the laser and molecular beams by a static electric field. A system of two electrostatic lenses provides space-focusing conditions for a range of acceleration voltages. After traversing an 18-cm field-free drift region, the ions reach a multichannel plate detector (MCP, Galileo, 25 nm) installed at the top of the TOF tube.

The polarization of the pump laser is controlled by a photoelastic modulator (PEM-80, HINDS International, Inc.). All TOF distributions are recorded with two polarizations (parallel and perpendicular to the TOF axis), which allows calculation of the recoil anisotropy parameter β.[38]

Because the ion signals are low, proper core sampling of the ion velocity distribution is impossible to achieve. Instead, the voltages applied to the extractor and repeller plates are gradually decreased while preserving space-focusing conditions. At the lowest possible voltage with an acceptable signal-to-noise ratio the MCP collects all ions with a perpendicular component of translational energy (E_t) lower than 0.6 eV, whereas increasingly better discrimination against ions with velocity components not aligned with the TOF axis is achieved at higher E_t. Under these conditions, an accurate center-of-mass (c.m.) E_t distribution of photofragments cannot be obtained without a deconvolution procedure. However, it is still possible to correctly determine the maximum translational energy, $E_{t,max}$, and identify different dissociation pathways that have distinct E_t distributions. In order to find the position and width of the peak in the region of low E_t, the experimental TOF spectrum was fitted with a spectrum calculated from a model velocity distribution composed of two Gaussian-like distributions. This method is described in more detail by Syage.[38] The conversion of the TOF spectra to an E_t scale is calibrated using E_t distributions obtained in our previous experiments on CH₂OH photodissociation.[28]

III. Results

Two types of experiments were carried out. First, REMPI and photofragment yield spectra of H or D were recorded in regions where transitions to Rydberg states were expected in
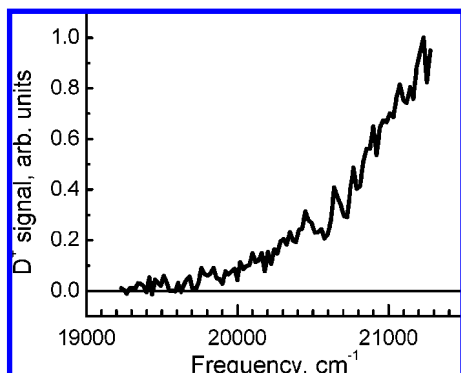
Figure 1. D photofragment yield spectrum of CH_3CHOD in the region $19\,000-21\,500$ cm^{-1}. Background signal is subtracted, and the signal is normalized to the OPO/OPA laser energy.

Figure 2. (Top) $2 + 1$ REMPI of CH_2OH in the region of absorption to the $3p_z$ state (adapted from ref 30). (Bottom) $2 + 2$ REMPI of CH_3-CHOH in the region of absorption to the $3p_z$ state. The lowest energy band of each transition is the origin band.

Figure 3. H fragment TOF spectrum from CH_3CHOH obtained at $21\,276$ cm^{-1} excitation. The polarization of the pump laser is alternated between parallel (solid line) and perpendicular (dashed line) to the TOF axis. The background is subtracted. Zero time indicates fragment with no recoil.

Figure 4. The c.m. E_t distribution obtained by monitoring H photofragments from CH_3CHOH following the $1^2A''(3s) \leftarrow 1^2A''$ transition at $21\,276$ cm^{-1}.(2.63 eV). The arrow indicates the available energy. The β parameter is plotted as a function of E_t in the top panel.

order to assign the electronic transitions. To elucidate the photodissociation dynamics, TOF spectra were obtained at selected energies, and the recoil anisotropy parameters were determined.
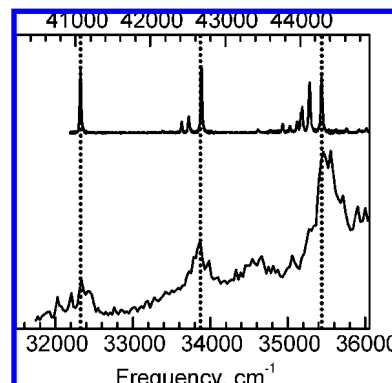
1. Photofragment Yield and REMPI Spectra. As stated in section I, our search for electronic absorption was guided by results obtained for CH_2OH.[30,33-35] In analogy with CH_2OH, we assumed that the lowest absorption bands involved Rydberg states and that the quantum defects did not change much relative to those in CH_2OH. As described in section IV, this was indeed found to be true, and therefore in the material that follows we use spectroscopic assignments of the upper electronic states that correspond to those in CH_2OH.

3s Region. This is the lowest excited state, and as in CH_2-OH,[34] no ions of CH_3CHOH (CH_3CHOD) were detected upon excitation in this region. Therefore, H(D) photofragment yield spectroscopy was used to monitor absorption. The onset of H (or D from CH_3CHOD) fragment signal was determined at $19\,600 \pm 100$ cm^{-1} (2.43 ± 0.01 eV). Figure 1 displays a background-subtracted D-photofragment yield spectrum in the region where the transition to the 3s Rydberg state was predicted to be located. A similar spectrum was obtained by monitoring H-fragments from CH_3CHOH, but the signal-to-noise ratio was slightly better with CH_3CHOD due to lower D background. No H signal from CH_3CHOD was observed in this region.
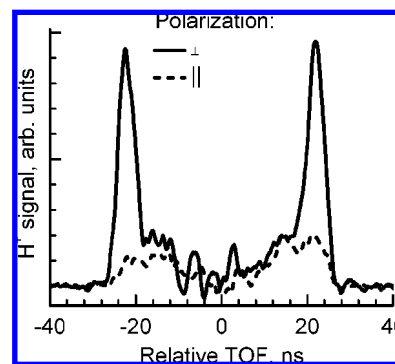
$3p_x$ Region. A distinct feature of the $3p_x$ state in CH_2OH was a longer lifetime than the 3s state, which has made REMPI detection possible.[34] In contrast, in CH_3CHOH, no REMPI signal was observed up to the origin band of the $3p_z$ state (see below). Photofragment yield spectra of H atoms taken in the wavelength region where absorption to $3p_x$ was expected did not show features that could distinguish it from absorption to the 3s state. Therefore, this transition remains unassigned.

$3p_z$ Region. A distinct $2 + 2$ REMPI spectrum was observed in the $32\,000-38\,000$ cm^{-1} region expected for the transition to the $3p_z$ state. The lowest energy peak in Figure 2 is assigned as the origin band of the transition, which is located at $32\,360 \pm 70$ cm^{-1} (4.01 ± 0.01 eV). Similar to the corresponding CH_2-OH spectrum shown in the top panel of Figure 2,[30] the two other peaks, located at 1560 ± 100 cm^{-1} intervals, form a vibrational progression in the C−O stretch excitation. The scan was taken with a step size of 5 cm^{-1}, but no additional structure was observed with a finer step size. The REMPI spectrum extends to shorter wavelengths than displayed in Figure 2, but no further structure is observed, probably due to a combination of spectral congestion and lifetime broadening.
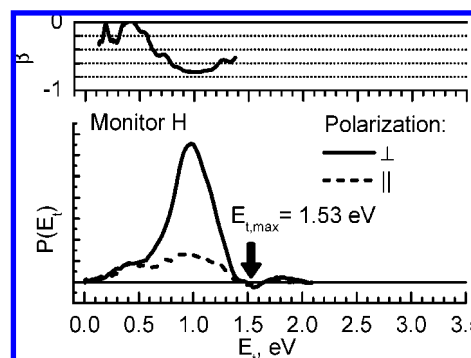
2. Time-of-Flight (TOF) of H(D) Photofragments. Figure 3 displays a typical background-subtracted TOF spectrum of H

atoms recorded following excitation at $21\,212$ cm^{-1} (2.63 eV; 470 nm) with laser polarization parallel and perpendicular to the ion TOF axis. The corresponding E_t distribution and the recoil anisotropy parameter $\beta(E_t)$ are shown in Figure 4. The maximum available energy is determined by energy conservation: $E_{avail} = E_{h\nu} + E^p_{int} - D_0$. The parent internal energy, E^p_{int}, is negligible in the supersonic expansion, and we use $E_{h\nu} = 2.63$ eV. From Figure 4 we obtain the maximum observed E_t: $E_{t,max} = E_{avail} = 1.53 \pm 0.1$ eV, which leads to $D_0 = 1.1 \pm 0.1$ eV, in good agreement with previous experimental and theoretical estimates (1.13 ± 0.04 eV and 1.04 eV, respectively).[21,25,39] The same D_0 value is obtained from $E_{t,max}$ at other wavelengths near the onset of the transition to the 3s

The 1-Hydroxyethyl Radical CH₃CHOH

J. Phys. Chem. A, Vol. 112, No. 3, 2008 **415**
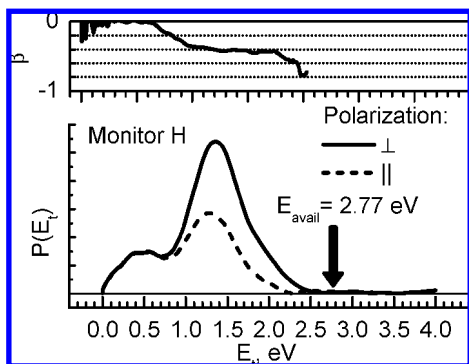
Figure 5. The c.m. E_t distribution obtained by monitoring H photofragments following excitation of CH₃CHOH at 31 250 cm^{-1} (3.87 eV). The arrow indicates the available energy. The β parameter is plotted as a function of E_t in the top panel.
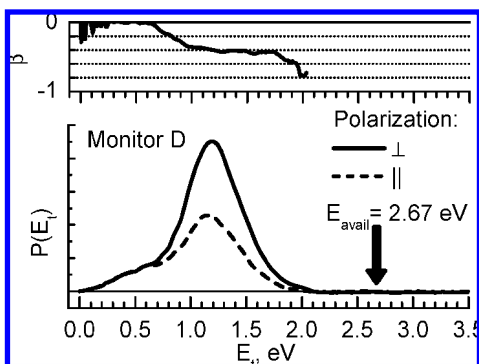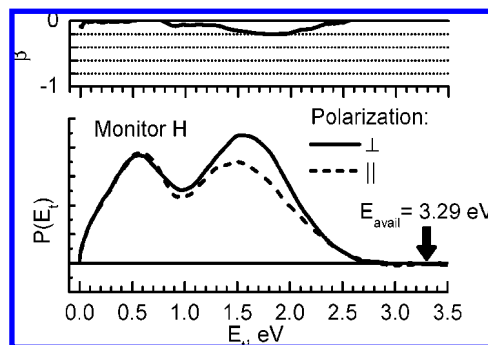

Figure 6. The c.m. E_t distribution obtained by monitoring D photofragments following excitation of CH₃CHOD at 31,250 cm^{-1} (3.87 eV). The arrow indicates the available energy. The β parameter is plotted as a function of E_t in the top panel.

Figure 7. The c.m. E_t distribution obtained by monitoring H photofragments following excitation of CH₃CHOH at 35 460 cm^{-1} (4.39 eV). The arrow indicates the available energy. The β parameter is plotted as a function of E_t in the top panel.

Figure 8. The c.m. E_t distribution obtained by monitoring D photofragments following excitation of CH₃CHOD at 35 460 cm^{-1} (4.39 eV). The arrow indicates the available energy. The β parameter is plotted as a function of E_t in the top panel.

Figure 9. Recoil anisotropy parameter β as a function of excitation energy.

state. The photofragment E_t distribution exhibits a single anisotropic peak with $\beta = -0.7 \pm 0.1$

Figure 5 displays the c.m. E_t distribution obtained by monitoring H fragments from photodissociation of CH₃CHOH at 31 250 cm^{-1} (3.87 eV) excitation energy with parallel and perpendicular polarizations of the pump laser. For high E_t the recoil distribution is anisotropic but with a lower anisotropy parameter than was observed at lower excitation energies (near the onset of absorption to the 3s state), and $\beta = -0.4 \pm 0.1$ is obtained for both CH₃CHOH and CH₃CHOD. In addition, a small isotropic peak ($\beta = -0.0 \pm 0.1$) appears in the low E_t region. The peak of slow photofragments is absent in Figure 6, which shows an E_t distribution for CH₃CHOD dissociation obtained at the same excitation energy by recording the D fragment TOF spectrum. A notable feature of this distribution is the difference between $E_{t,max}$ and the available energy: $E_{avail} = E_{h\nu} - D_0 = 3.87 - 1.2 = 2.67 \pm 0.1$ eV (where D_0 is adjusted for zero-point energy), whereas $E_{t,max} = 2.2 \pm 0.1$ eV, giving, $E_{avail} - E_{t,max} = 0.47 \pm 0.14$ eV as the minimum internal energy in the molecular cofragment. In contrast, in the case of CH₃CHOH, $E_{t,max}$ and E_{avail} are equal within the error bars. H and D fragment TOF spectra in the 21 000−31 300 cm^{-1} excitation range show similar trends.
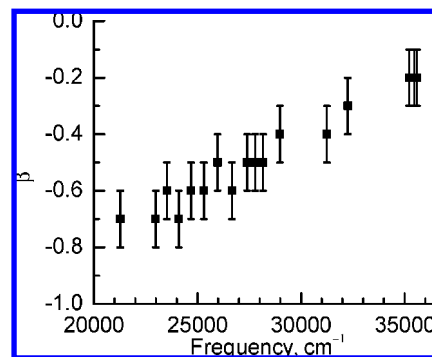
Figures 7 and 8 show typical c.m. E_t distributions obtained following excitation of CH₃CHOH (CH₃CHOD) at 35 460 cm^{-1} (the third peak in Figure 2). The two peaks in Figure 7 become broader than those at lower excitation energy, and the recoil anisotropy parameters of the high E_t peaks are lower ($\beta = -0.2 \pm 0.1$). The low E_t peak grows in relative intensity but remains isotropic. The gap between $E_{t,max}$ and E_{avail} increases to 0.39 eV (0.79 eV) for CH₃CHOH (CH₃CHOD). The $E_{t,max} - E_{avail}$
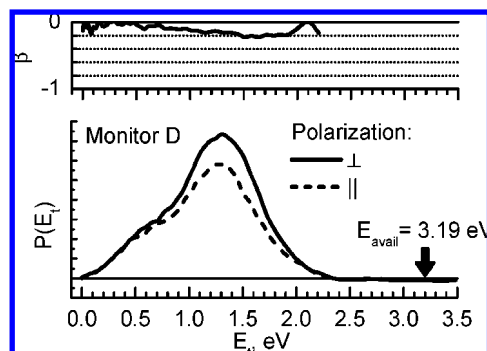
gap increases gradually with excitation energy up to the highest measured excitation energy of 35 460 cm^{-1}, while the β parameter decreases with increasing excitation energy. The dependence of β on excitation energy is shown in Figure 9. A TOF distribution was also recorded by monitoring D atoms from the CD₃CHOH isotopolog. It showed only a slow peak comparable to the low E_t peak in Figure 7, in contrast to the D fragment TOF spectrum from CH₃CHOD, which displayed only the high E_t peak.

IV. Discussion

1. Assignment of the 3s and 3p$_z$ States. The low ionization energy of CH₂OH results in electronic Rydberg states that are lower in energy than the lowest valence states.[32,36,40] Since the ionization energy of CH₃CHOH is almost 1 eV lower than that of CH₂OH (6.64 eV vs 7.56 eV),[25,26] the lowest-lying electronic

states of the former are also expected to be of Rydberg nature and lie at even lower excitation energy. The valence states, however, should not vary much in energy in going from CH_2-OH to CH_3CHOH. The positions of the Rydberg states can be estimated by the Rydberg formula: $E = IE - R/(n - \delta)$,[2] where $R = 109\ 737.316\ cm^{-1}$, n is the principal quantum number, and δ is the quantum defect obtained experimentally from the energies of the corresponding Rydberg states of CH_2OH (see Table 1).

The first excited electronic state is the 3s state. The onset of the H photofragment yield spectrum is at $19\ 600 \pm 100\ cm^{-1}$, which is close to the predicted value of $18\ 530\ cm^{-1}$. Our inability to observe a CH_3CHOH^+ REMPI signal despite the stability of the ion[12,14] suggests that internal conversion from the 3s to the ground state with subsequent dissociation is faster than ionization from the Rydberg state. A similar conclusion was reached with regard to CH_2OH in the 3s state.[29,34] Notice that CH_3CHOH starts absorbing at 510 nm, which makes it unstable in visible light.

Another feature common to CH_2OH and CH_3CHOH is the strong negative recoil anisotropy of the photofragment distribution in excitation to the 3s state ($\beta_{3s} = -0.7 \pm 0.1$ for both radicals near the onset of the transition). The ground-state equilibrium geometry of both CH_2OH and CH_3CHOH is nonplanar.[12,14] In CH_2OH, a low barrier to CH_2 inversion (140 cm^{-1}) allows the two mirror image equilibrium structures of C_1 symmetry to rapidly interconvert.[41−43] As a result, the electronic wavefunction of CH_2OH complies with the C_s point group. This gives the transition from the ground state (A″) to the 3s and $3p_x$ states, which are of A′ symmetry, a perpendicular moment. The observation of similar anisotropy in the transition to 3s for both radicals suggests similar orientation of the transition dipole moment relative to the O−H bond (the only bond fission channel observed near the onset of 3s state excitation) as well as similar symmetry of the electronic wavefunctions. By use of C_s symmetry for the electronic transitions of CH_3CHOH, we assign the first two Rydberg states as $1^2A'(3s)$ and $2^2A'(3p_x)$. For CH_2OH, the transition to $3p_y$ was calculated to be very weak and was not observed;[31,40] likewise, we do not see any evidence for a transition to this state in CH_3CHOH.

The $3p_x$ state of CH_3CHOH could not be identified in our experiment. No REMPI of CH_3CHOH was seen around the predicted onset of the transition (about $27\ 700\ cm^{-1}$), and no discernible change in the H-photofragment spectrum was detected. In the hydroxymethyl radical, fast predissociation of the $3p_x$ state caused considerable broadening of the peaks in the REMPI spectrum.[34] Since CH_3CHOH has twice as many vibrational degrees of freedom as CH_2OH, it is likely that the $3p_x$ state predissociates even faster, reducing its ionization efficiency and broadening the peaks beyond the sensitivity of our measurements. Apparently, H-photofragment spectra in this excitation region are dominated by 3s state absorption and show no special features that indicate the onset of additional absorption to another state.

The first REMPI signal of CH_3CHOH appears at $32\ 360$ cm^{-1}, near the predicted origin of absorption to the $3p_z$ ($2^2A''$) state at $33\ 684\ cm^{-1}$. In keeping with a model of faster predissociation than in CH_2OH, the peaks are much broader than for the $3p_z$ state of CH_2OH (Figure 2). As in hydroxymethyl, they form a vibrational progression with peaks separated by $1560 \pm 100\ cm^{-1}$, close to the frequency of the C−O stretch vibration in the ion.[25] The progression can be rationalized by the promotion of an electron from the C−O antibonding π^*

orbital to a nonbonding Rydberg orbital in excitation to the $3p_z$ state, which leads to a shortening of the C−O bond length. In contrast to the H photofragment yield spectrum of CH_2OH in the region of the $3p_z$ state, which shows the same vibronic bands as the REMPI spectrum, there was no discernible structure in the H(D) yield spectra of $CH_3CHOH(D)$ above the onset of the transition to $3p_z$, indicating that absorption to the 3s state still dominates the absorption spectrum in this region.

It is noteworthy that a 2 + 1 REMPI spectrum of CH_3CHOH was reported in the region around 430−460 nm ($2h\nu = 46\ 510-$ $43\ 480\ cm^{-1}$),[24] which corresponds according to the Rydberg formula to one of the 4p states. Higher Rydberg states usually couple less efficiently to other Rydberg and valence states, and their dissociation is less rapid, which allows observation of the 2 + 1 REMPI signal.

2. Photodissociation Dynamics. The conclusion from the spectroscopic studies is that, throughout the examined region, which encompasses absorptions to the 3s, $3p_x$, and $3p_z$ Rydberg states, the predominant absorption is to the 3s state. Therefore, in the discussion below, we assume that dissociation is initiated from 3s, although contributions from $3p_x$ excitation are likely at shorter wavelengths.

The ground state of the CH_3CHOH^+ ion is bound, and therefore so are the Rydberg states of the neutral, provided they do not interact with other states. As Rydberg states correlate with excited-state products, the 3s Rydberg state, which is the lowest electronic state, must couple to the ground state in order to predissociate to ground-state products. Near the onset of the 3s state, dissociation channels (1) and (2) are energetically accessible; i.e., both the O−H ($D_0 = 1.04$ eV) and the $C^{(2)}$−H ($D_0 = 1.46$ eV) bond fission channels,[21] where $C^{(2)}$ is the terminal carbon atom, are allowed. Both channels have similar barrier heights on the ground state PES (calculated at 1.52 and 1.58 eV, respectively).[21]

Had internal conversion from 3s to the ground state been followed by statistical redistribution of energy among the vibrational modes on the ground PES, one would expect close competition between these two simple bond fission channels above the barrier. However, the E_t distribution near the onset of the absorption to 3s is clearly nonstatistical as most of E_{avail} is deposited in translation. Also, only the O−H bond fission channel (1) is detected, even though channel (2) is energetically accessible. This follows from a comparison of the E_t distributions obtained by monitoring H and D fragments from dissociation of CH_3CHOH and CH_3CHOD, respectively: each exhibits a single peak of the same shape, with $E_{t,max} = E_{avail}$ corresponding to $D_0 = 1.1 \pm 0.1$ eV.

At 3.87 eV ($31\ 250\ cm^{-1}$) excitation, however, a second dissociation channel is open, as seen in the H-fragment E_t distribution of Figure 5. It exhibits an additional peak in the region of low E_t, which is not present in the corresponding D fragment E_t distribution (Figure 6). Deconvolution of the H fragment TOF spectrum obtained by assuming two Gaussian-shape distributions of E_t (section II) shows that the channel represented by the slow peak must have $D_0 < 2.7 \pm 0.1$ eV. This value is larger than the calculated D_0 value of the $C^{(2)}$−H bond fission (1.46 eV) but smaller than D_0 for $C^{(1)}$−H bond fission (calculated at 3.37 eV).[21,27] The interpretation that the low E_t peak arises from channel (2) giving rise to CH_2CHOH product agrees with the result of the D fragment TOF spectrum of CD_3CHOH, which showed only the low E_t peak. Unfortunately, the core-sampling assumption breaks at low E_t, so the slow peak in the TOF spectrum cannot be analyzed quantitatively. We can say, however, that the $C^{(2)}$−H bond fission

The 1-Hydroxyethyl Radical CH₃CHOH

J. Phys. Chem. A, Vol. 112, No. 3, 2008 **417**

channel opens >1 eV higher than the O−H bond fission channel, despite the similar barrier heights of the two reactions on the ground state PES. We conclude, therefore, that the dynamics on the 3s state PES must be responsible for this difference.

In CH_2OH, calculations identified an efficient (vertical) conical intersection between the 3s and the ground state, which was located in the PES region of elongated O−H bond.[36,37] This geometry favors fast and efficient dissociation of the O−H bond. A second conical intersection, located at much higher energies, led to C−H bond fission.[36,37] It is reasonable to assume that in CH_3CHOH there are at least two conical intersections between the 3s and the ground state, each favoring one of the two exit channels. Thus, after the radical goes through the conical intersection it dissociates predominantly through the corresponding channel. Accessibility to the dissociation channel in each case is controlled by the nuclear geometry and minimum energy of the intersection on the 3s PES.

In reference to the properties of the conical intersection, it appears that certain vibrations must be active for efficient surface coupling to take place. As the excitation energy increases in the ground-state PES following internal conversion, an increasing fraction of the parent vibrational energy is deposited into modes that appear finally as internal modes (vibration and rotation) of the acetaldehyde fragments. This is manifested in the broadening of the high-energy peak in the E_t distributions and the increasing value of $E_{avail} - E_{t,max}$. The latter is especially pronounced in CH_3CHOD. The slow vinyl alcohol product from channel (2) also has a broad internal energy distribution.

It appears that some of the excited parent vibrational levels involve out-of-plane motions, which reduce the recoil anisotropy in the perpendicular transition. Indeed, the recoil anisotropy parameter β becomes less negative as the excitation energy increases (Figure 9), concomitant with the internal energy buildup in the products. This effect is much less noticeable in $CH_2OH(D)$ where the β parameter is nearly constant over the entire range of perpendicular transitions to 3s and 3p$_x$, and a sudden change in anisotropy occurs only at the onset of the parallel transition to the Rydberg 3p$_z$ state.[28,30,34] The observation of an isotropic energy distribution for channel (2) may also reflect the favored geometries that lead to nonadiabatic transitions. The C−H bond fission channel in CH_2OH was also isotropic.[29]

V. Conclusions

Electronic transitions to low-lying Rydberg states and photodissociation dynamics of the $CH_3CHOH(D)$ radical in the region 19 600−37 000 cm⁻¹ were studied for the first time in a molecular beam. On the basis of the REMPI and H(D) photofragment yield spectra, we conclude that the predominant absorption in the observed region is to the lowest excited state—the Rydberg 3s state—whose onset is at 19 600 cm⁻¹. The origin band of the transition to the 3p$_z$ state lies at 32 360 cm⁻¹. The onsets of the observed absorptions agree well with predictions obtained by using the Rydberg formula with quantum defects similar to those obtained for the corresponding transitions in CH_2OH.

To identify the photodissociation channels, TOF spectra of D and H photofragments were recorded for CH_3CHOH, CH_3CHOD, and CD_3CHOH. At dissociation energies near the onset of absorption to the 3s state, c.m. fragment E_t distributions from CH_3CHOH show only one peak at high E_t, close to the maximum allowed by energy, with a recoil anisotropy parameter β typical of a perpendicular transition. At higher excitation

energies, a second, low E_t peak appears, which is isotropic; its relative intensity increases at higher excitation energies.

The TOF spectra obtained with the three isotopologs allow us to identify two independent dissociation channels, one leading to acetaldehyde and the other to vinyl alcohol (enol): (1) $CH_3CHO + H$; and (2) $CH_2CHOH + H$. There is no indication of isomerization to ethoxy. The former channel appears at the onset of the 3s absorption, whereas the latter first appears only ∼1 eV above its thermochemical threshold. We suggest that conical intersections with the ground state lead to O−H bond fission [channel (1)] from the onset of absorption to 3s, but the conical intersection leading to the enol product [channel (2)] has a minimum energy much above the thermochemical threshold for this channel.

Another notable feature of the dissociation is the increasing amount of internal energy in acetaldehyde [channel (1)] as the excitation energy increases. The less negative β of the fast peak at higher excitation energies may result from out-of-plane motions during dissociation of vibrationally excited molecules generated in the nonadiabatic transition with the ground electronic state. These results reflect the dynamics in the region of the conical intersections as well as dynamics in the exit channel.

From experiment and theory we conclude that the Rydberg formula should hold rather well in the homologous series of CH_2OH, serving as a guide to the absorption spectra of higher hydroxyalkyl radicals whose radical center is located on the C adjacent to OH (1-position). The structureless electronic absorption extends from the visible to the UV, making these radicals unstable to visible light. Also, nonadiabatic transitions coupling the Rydberg states to the ground state are expected to be efficient, resulting in fast dissociation to several product channels.

References and Notes

(1) Lin, J. J.; Harich, S.; Lee, Y. T.; Yang, X. *J. Chem. Phys.* **1999**, *110*, 10821.
(2) Lin, J. J.; Shu, J.; Lee, Y. T.; Yang, X. *J. Chem. Phys.* **2000**, *113*, 5287.
(3) Fockenberg, C.; Hall, G. E.; Preses, J. M.; Sears, T. J.; Muckerman, J. T. *J. Phys. Chem. A* **1999**, *103*, 5722.
(4) Marcy, T. P.; Diaz, R. R.; Heard, D.; Leone, S. R.; Harding, L. B.; Klippenstein, S. J. *J. Phys. Chem. A* **2001**, *105*, 8361.
(5) Seakins, P. W.; Leone, S. R. *J. Phys. Chem.* **1992**, *96*, 4478.
(6) Ahmed, M.; Peterka, D. S.; Suits, A. G. *Phys. Chem. Chem. Phys.* **2000**, *2*, 861.
(7) Pagsberg, P.; Munk, J.; Anastasi, C.; Simpson, V. J. *J. Phys. Chem.* **1989**, *93*, 5162.
(8) Pagsberg, P.; Munk, J.; Sillesen, A.; Anastasi, C. *Chem. Phys. Lett.* **1988**, *146*, 375.
(9) Rudic, S.; Murray, C.; Ascenzi, D.; Anderson, H.; Harvey, J. N.; Orr-Ewing, A. J. *J. Chem. Phys.* **2002**, *117*, 5692.
(10) Anastasi, C.; Simpson, V.; Munk, J.; Pagsberg, P. *Chem. Phys. Lett.* **1989**, *164*, 18.
(11) Anastasi, C.; Simpson, V.; Munk, J.; Pagsberg, P. *J. Phys. Chem.* **1990**, *94*, 6327.
(12) Curtiss, L. A.; Lucas, D. J.; Pople, J. A. *J. Chem. Phys.* **1995**, *102*, 3292.
(13) Ruscic, B.; Berkowitz, J. *J. Chem. Phys.* **1994**, *101*, 10936.
(14) Nobes, R. H.; Rodwell, W. R.; Bouma, W. J.; Radom, L. *J Am. Chem. Soc.* **1981**, *103*, 1913.
(15) Choi, H.; Bise, R. T.; Neumark, D. M. *J. Phys. Chem. A* **2000**, *104*, 10112.

(16) Faulhaber, A. E.; Szpunar, D. E.; Kautzman, K. E.; Neumark, D. M. *J. Phys. Chem. A* **2005**, *109*, 10239.

(17) Taatjes, C. A.; Christensen, L. K.; Hurley, M. D.; Wallington, T. J. *J. Phys. Chem. A* **1999**, *103*, 9805.

(18) Cleary, P. A.; Romero, M. T. B.; Blitz, M. A.; Heard, D. E.; Pilling, M. J.; Seakins, P. W.; Wang, L. *Phys. Chem. Chem. Phys* **2006**, *8*, 5633.

(19) Hoyermann, K.; Olzmann, M.; Seeba, J.; Viskolcz, B. *J. Phys. Chem. A* **1999**, *103*, 5692.

(20) Lindner, J.; Loomis, R. A.; Klaassen, J. J.; Leone, S. R. *J. Chem. Phys.* **1998**, *108*, 1944.

(21) Senosiain, J. P.; Klippenstein, S. J.; Miller, J. A. *J. Phys. Chem. A* **2006**, *110*, 6960.

(22) Tully, F. P. *Chem. Phys. Lett.* **1988**, *143*, 510.

(23) Taatjes, C. A.; Hansen, N.; McIlroy, A.; Miller, J. A.; Senosiain, J. P.; Klippenstein, S. J.; Qi, F.; Sheng, L. S.; Zhang, Y. W.; Cool, T. A.; Wang, J.; Westmoreland, P. R.; Law, M. E.; Kasper, T.; Kohse-Hoinghaus, K. *Science* **2005**, *308*, 1887.

(24) Edelbuttel-Einhaus, J.; Hoyermann, K.; Rohde, G.; Seeba, J. *Proceedings of the 24th Symposium International on Combustion*; Combustion Institute: Pittsburgh, PA, 1992; p 661.

(25) Dyke, J. M.; Groves, A. P.; Lee, E. P. F.; Niavaran, M. H. Z. *J. Phys. Chem. A* **1997**, *101*, 373.

(26) Dyke, J. M.; Ellis, A. R.; Jonathan, N.; Keddar, N.; Morris, A. *Chem. Phys. Lett.* **1984**, *111*, 207.

(27) Klippenstein, S. Private communication.

(28) Feng, L.; Demyanenko, A. V.; Reisler, H. *J. Chem. Phys.* **2003**, *118*, 9623.

(29) Feng, L.; Demyanenko, A. V.; Reisler, H. *J. Chem. Phys.* **2004**, *120*, 6524.

(30) Aristov, V.; Conroy, D.; Reisler, H. *Chem. Phys. Lett.* **2000**, *318*, 393.

(31) Bruna, P. J.; Grein, F. *J. Phys. Chem. A* **1998**, *102*, 3141.

(32) Bruna, P. J.; Grein, F. *J. Phys. Chem. A* **2001**, *105*, 8599.

(33) Conroy, D.; Aristov, V.; Feng, L.; Reisler, H. *J. Phys. Chem. A* **2000**, *104*, 10288.

(34) Feng, L.; Huang, X.; Reisler, H. *J. Chem. Phys.* **2002**, *117*, 4820.

(35) Feng, L.; Reisler, H. *J. Phys. Chem. A* **2004**, *108*, 9847.

(36) Hoffman, B. C.; Yarkony, D. R. *J. Chem. Phys.* **2002**, *116*, 8300.

(37) Yarkony, D. R. *J. Chem. Phys.* **2005**, *122*.

(38) Syage, J. A. *J. Chem. Phys.* **1996**, *105*, 1007.

(39) Lias, S. G.; Bartmess, J. E.; Liebman, J. F.; Holmes, J. L.; Levin, R. D.; Mallard, W. G. *J. Phys. Chem. Ref. Data* **1988**, *17*, 1.

(40) Rettrup, S.; Pagsberg, P.; Anastasi, C. *Chem. Phys* **1988**, *122*, 45.

(41) Marenich, A. V.; Boggs, J. E. *J. Chem. Phys.* **2003**, *119*, 10105.

(42) Marenich, A. V.; Boggs, J. E. *J. Chem. Phys.* **2003**, *119*, 3098.

(43) Johnson, R. D.; Hudgens, J. W. *J. Phys. Chem.* **1996**, *100*, 19874.